Fabrication and Transport Critical Current Densities of MgB_2/Fe/Cu Multifilament Tapes without Any Intermediate Annealing

E. Yucel[a,*], C. Terzioglu[b], A. Varilci[b], A. Gencer[c] and I. Belenli[b]

[a]Department of Physics, Faculty of Arts and Sciences, Mustafa Kemal University, 31034 Hatay, Turkey

[b]Department of Physics, Faculty of Arts and Sciences, Abant Izzet Baysal University, 14280 Bolu, Turkey

[c]Department of Physics, Faculty of Science, Ankara University, 06100 Ankara, Turkey

(Received May 31, 2011; in final form December 8, 2011)

We have fabricated superconducting 6 and 7 filaments MgB_2/Fe/Cu tapes by *ex situ* powder-in-tube method using Cu-sheath without any intermediate annealing. Properties of two different multicore MgB_2/Fe/Cu tapes annealed at 900 °C for 2 h in high purity argon gas atmosphere were compared. The samples were characterized using scanning electron microscope, X-ray diffraction, electron dispersive spectroscopy, optical microscopy, critical transition temperature, transport critical current density, and magnetic measurements. Transport critical current densities of the 6 and 7 filaments tapes were found to be 450 A/cm^2 and 190 A/cm^2 at 20 K, respectively. From X-ray diffraction measurements, lattice parameters a and c were determined. From dc resistivity measurements, the connectivity between grains was investigated by using Rowell's connectivity analysis.

PACS: 74.70.Ad, 84.71.Mn, 74.62.−c, 74.25.Sv, 74.25.F−

1. Introduction

The discovery of superconductivity at 39 K in MgB_2 compound by Akimitsu's group [1] has created great interests worldwide in both theoretical studies and potential applications. Compared with high temperature superconductors (HTS), MgB_2 compound has simple structure, light weight, high abundance of Mg and B, low anisotropy, large coherence lengths and absence of weak-link. Due to its properties, MgB_2 material is interesting for potential applications such as magnetic resonance imaging (MRI) and transformers at operating temperature of 20–30 K [2–6].

Powder in tube (PIT) method is most preferred for the preparation of MgB_2 superconducting wires and tapes. There are two processes for fabricating MgB_2 wires and tapes using the PIT method which is known as *ex situ* and *in situ* methods. Many research groups have already made a lot of studies concerning the fabrication of superconducting MgB_2 wires and tapes by both *in situ* and *ex situ* PIT method [3–14]. In the *ex situ* method, fabrication of MgB_2 wires and tapes is made by using MgB_2 reacted powder [7–10] while, in the *in-situ* method, fabrication of MgB_2 wires and tapes is made by using a mixture of Mg and B powder with stoichiometric composition [11–14]. In PIT method, the packing density of MgB_2 powder is very important to obtain a high critical current density (J_c) [15]. Several metals and alloys have been found to be suitable as sheath materials such as Fe [16], Cu [17], Ag [18], Fe/stainless steel [19], Cu–Ni [20, 21] and CuSn [22] in the PIT method. Sheath materials should be ductile for mechanic deformation and should not react with Mg and hence degrade the superconducting properties [16]. For technical applications of the MgB_2 wires and tapes, good thermal and mechanical stability of the conductor is necessary. In order to increase the thermal stability, conductive metals Cu or pure Al can be added to the sheath composite acting as parallel shunt [22, 23]. Cu is an ideal stabilizing metal for low T_c superconducting wires and tapes. Copper is advantageous for its low resistance and weak paramagnetic properties but Cu reduces J_c values of the MgB_2 composite wire since it reacts with MgB_2 core [24]. The Fe is generally used as a reaction barrier between Cu stabilization material and MgB_2 core [25]. Moreover, iron is the most suitable sheath material due to its chemical compatibility with the MgB_2 core and good mechanical stability [4, 26–29].

In this paper, we report on the fabrication and superconducting properties of multifilamentary tapes prepared with and without copper core by *ex situ* PIT method using Cu sheath without any intermediate annealing.

* corresponding author; e-mail: ersin_yucel@msn.com

2. Experimental

MgB_2 superconducting samples were fabricated by *ex situ* PIT method using commercially available MgB_2 powder (Alfa Aesar, -325 mesh, < 44 μm) without any intermediate annealing. The MgB_2 powder was filled into a 17 cm long pure Fe tube whose one end is sealed with an outside diameter of 4.95 mm and wall thickness of 0.3 mm and tightly packed. This packing process was carried out in high purity argon gas atmosphere inside the glove box. Then, the other end of the tube was sealed by silver plug. After sealing both ends of tube, it was cold drawn in a number of steps with about 5% of cross-section reduction to an outer diameter of 1.52 mm without any intermediate annealing. After that, six pieces of the Fe clad wire, each about 15 cm in length, were stacked inside into the copper tube in a multifilamentary geometry, which also included an inner copper core in a high purity argon gas atmosphere inside the glove box. After sealing both ends of copper tube, it was cold drawn in a number of steps with about 5% of cross-section reduction to an outer diameter of 2.46 mm without any intermediate annealing. In order to prevent contamination of the MgB_2 filaments by copper, an iron diffusion barrier was used. The multifilament wires were fabricated with and without copper core by *ex situ* PIT method. The seven filaments MgB_2 wire was fabricated by similar process. Finally, six and seven filaments MgB_2 tapes were fabricated by cold rolling. The samples of MgB_2 multifilamentary tapes will be hereafter denoted as M6A (MgB_2/Fe/Cu 6 filament tape non-annealed), M6B (MgB_2/Fe/Cu 6 filament tape annealed at 900 °C for 2 h), M7A (MgB_2/Fe/Cu 7 filament tape non-annealed), and M7B (MgB_2/Fe/Cu 7 filament tape annealed at 900 °C for 2 h). All heat treatments were carried out in high purity Ar gas atmosphere.

Resistivity measurements were carried out by standard four-probe method using Keithley nanovoltmeter (Model 2182A), current source (Model 238) and a constant DC bias current of 100 mA between 4 and 50 K temperatures in a cryostat. The active cross-sectional area fraction (A_F) values can be estimated from resistivity measurements by using Rowell's connectivity analysis [30],

$$A_F = \rho_{ideal}/[\rho_{300\,K} - \rho_{40\,K}], \tag{1}$$

where $\rho_{ideal} = 7.3$ $\mu\Omega$ cm [31, 32]. In addition, the residual resistivity ratio (RRR) is given by [33]:

$$RRR = \rho_{300\,K}/\rho_{40\,K}. \tag{2}$$

This value was estimated for each sample. The connectivity analysis measurements of the multifilament tapes were carried out with and without MgB_2 cores in the tapes thus the influence of Cu and Fe conductivities on the total conductivity of the tape were determined. Standard Pb–Sn (40/60) solder was used for forming the current and voltage contacts. Both of voltage contacts were directly soldered with standard Pb–Sn (40/60) solder to the sheath materials of the samples. Both ends of the samples were painted with silver and then both painted ends of the samples were soldered with standard Pb–Sn (40/60) solder for current contacts as shown in Fig. 1. The current–voltage (I–V) characteristics of the samples were measured at 20 K with the standard four-probe method under self-field. A Philip Harris current source, Lake Shore 331 temperature controller, Hewlett Packard 34401A multimeter and Leybold cryostat system were used for I–V measurements. The critical currents (I_c) were evaluated from I–V curves taking the electric field criterion of 1 μV/cm. The J_c was defined as I_c divided by the cross-section area of the MgB_2 core which was measured with a help of a scanning electron microscope.

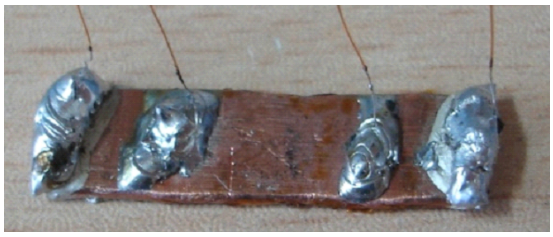

Fig. 1. Current and voltage contacts of MgB_2/Fe/Cu multifilamentary tape.

The surface morphologies of the multifilamentary MgB_2 samples were studied by using a JEOL JSM-6390 LV scanning electron microscope (SEM). SEM in a combination with an energy dispersive X-ray spectrometer (EDS) analysis was used for studying the chemical composition of the samples. The surface structures of the multifilamentary MgB_2 samples were investigated by OLYMPLUS GX41 optical microscope.

The phase composition and crystal structure investigation of the multifilamentary MgB_2 samples were characterized by XRD method using a Rigaku MultiFlex 2 kW X-ray diffractometer with Cu K_α radiation ($\lambda = 1.5418$ Å) in the range $2\theta = 3°-80°$ with a scan speed of 3°/min and a step increment of 0.02° at room temperature. Phase purity, lattice parameters and crystallite size were determined from these XRD patterns. The values of grain sizes can be estimated from XRD measurements by using the Scherrer–Warren formula [34]:

$$D = (0.94\lambda/B\cos\theta), \tag{3}$$

where D is the crystallite size in nm, λ (15.418 nm) is the wavelength of X-ray in nm, θ is the angle of intensity peak and B is the full width at half maximum (FWHM) of the same intensity peak.

Magnetic moment versus temperature properties were measured at 0.1 T between 10 K and 50 K by using a quantum design physical property measurement system (PPMS) under the zero field-cooling regimes (ZFC). The measurements were carried out by the sweep rate of 5 mT s^{-1}.

3. Results and discussion

Figure 2 shows SEM pictures of polished transverse cross-sections of six and seven filaments MgB_2/Fe/Cu wires and tapes without heat treatment. After cold drawing, the multifilamentary wires have uniform transversal sections and regular round shapes, as can be seen from the figure. The matrix metal of the multifilamentary wires is copper. A copper stabilizer is located in the six filaments MgB_2/Fe/Cu wire. Between MgB_2 and copper, an iron barrier is placed in order to prevent diffusion of copper to MgB_2 during heat treatment. However, after cold rolling, the six filaments tape has uniform deformation, as shown in Fig. 2c but the seven filaments tape does not exhibit well-distributed MgB_2 filaments, as shown in Fig. 2d. Cu stabilizer in the centre is helpful for obtaining evenly distributed filaments in tape making via rolling. Iron sheathing as barrier is also beneficial for the same purpose. Table I summarizes the main characteristics of the six and seven filaments wires.

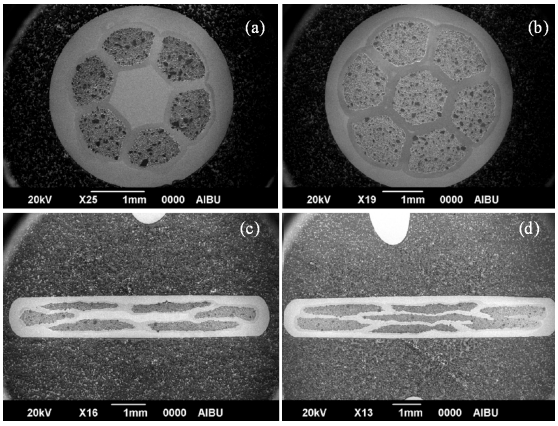

Fig. 2. SEM pictures of polished transverse cross-sections: (a) six filaments MgB_2/Fe/Cu wire, (b) seven filaments MgB_2/Fe/Cu wire, (c) six filaments MgB_2/Fe/Cu tape, (d) seven filaments MgB_2/Fe/Cu tape.

TABLE I
Six and seven filaments wire characteristics.

Number of MgB_2 filaments	6	7
preparation technique	*ex situ* PIT	*ex situ* PIT
sheath material	copper	copper
diffusion barrier material	iron	iron
composite (MgB_2/Fe/Cu) cross-section [mm^2]	9.18167	16.6106
MgB_2 cross-section [mm^2]	2.30790	5.49500
iron cross-section [mm^2]	0.70650	3.22886
copper cross-section [mm^2]	6.16727	7.88674

We have performed EDS measurements for elemental analysis as presented in Fig. 3. The figure shows Mg, B, Fe, Cu and O element composition mappings taken on the cross-section of the M6A, M6B, M7A and M7B

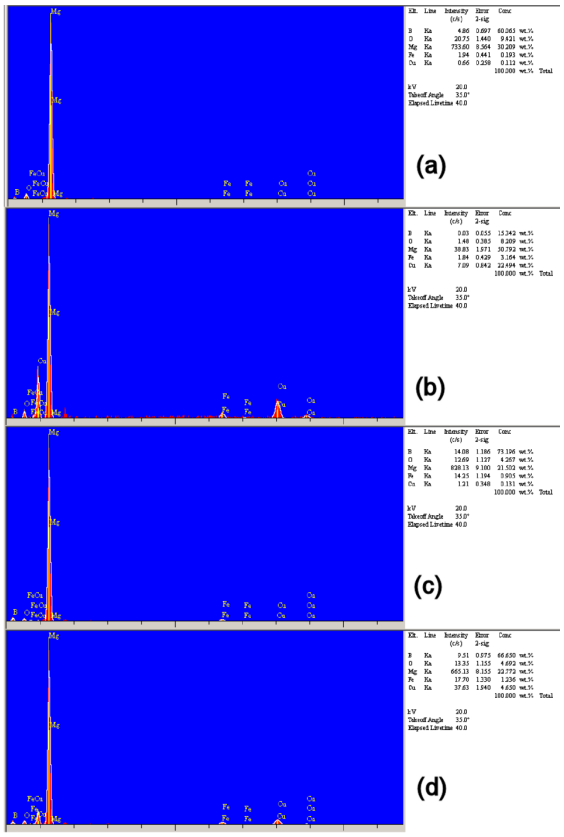

Fig. 3. EDS results of the samples: (a) M6A, (b) M6B, (c) M7A, and (d) M7B.

samples. As can be seen from the figure, we observed that the percentages of Mg in the M6B and M7B samples are higher than the M6A and M7A samples, respectively. On the other hand, we observed that the percentages of B in the M6B and M7B samples are lower than those of M6A and M7A samples, respectively. We think that the Mg in the M6B and M7B samples may have been collected in the cross-section area which was taken as EDS data after heat treatment.

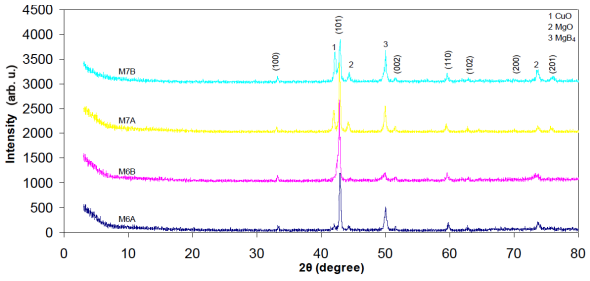

Fig. 4. X-ray diffraction patterns of the M6A, M6B, M7A, and M7B samples.

The phase compositions and microstructure properties of the samples were investigated by XRD measurements. Figure 4 shows intensities as a function of 2θ for the M6A,

M6B, M7A, and M7B samples. The Miller indices are indicated in the figure. The lattice parameters a and c determined from the (h00) and (00 l) peaks of the XRD data are given in Table II.

TABLE II

The lattice parameters a and c of the M6A, M6B, M7A and M7B samples.

Samples	a [Å]	c [Å]
M6A	3.0891	3.5271
M6B	3.0986	3.5392
M7A	3.0890	3.5265
M7B	3.0863	3.5247

The XRD pattern analysis of M6A, M6B, M7A, and M7B shows MgB_2 as a main phase and CuO, MgO, and MgB_4 as impurity phases. The XRD analysis shows that there are almost no reactions between MgB_2 and barrier materials. The crystallographic symmetry of the material was found to be hexagonal. An appreciable change in the lattice parameters of the samples was found within the experimental limit. Both lattice parameters a and c for the M6A and M6B samples increase slightly from 3.0891 to 3.0986 Å and from 3.5271 to 3.5392 Å with the heat treatment, respectively. On the other hand, both lattice parameters a and c for the M7A and M7B samples decrease from 3.0890 to 3.0863 Å and from 3.5265 to 3.5247 Å with the heat treatment, respectively.

Comparing the non-annealed and annealed samples, the peak (101) shifts to low angle for the sample M6B (annealed sample) while the peak (101) shifts to high angle for the sample M7B (annealed sample). Therefore, lattice parameters a and c increase with annealing for the sample M6B but these parameters decrease with annealing for the sample M7B. The grain sizes estimated from XRD measurements by the Scherrer–Warren formula are approximately 50–60 nm for all samples.

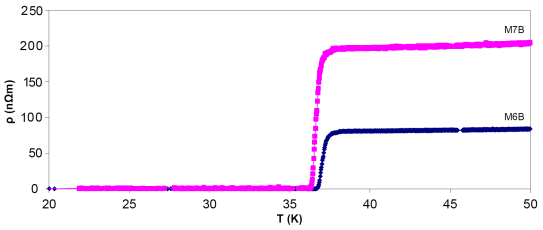

Fig. 5. Resistivity versus temperature graphs of the M6B and M7B samples.

The temperature dependence of the resistivity of the samples M6B and M7B is shown in Fig. 5. T_c^{onset}, T_c^{offset}, and ΔT_c values were tabulated in Table III.

The T_c^{offset} (K) values of the M6B and M7B samples were obtained as 36.7 K and 36.3 K, respectively. No difference between the M6B and M7B samples in transition width was observed.

TABLE III

The superconducting transition temperature values of the M6B and M7B samples.

Tapes	T_c^{onset} [K]	T_c^{offset} [K]	ΔT_c [K]
M6B	37.6	36.7	0.9
M7B	37.2	36.3	0.9

The active cross-sectional area fraction values were estimated from resistivity measurements by using Rowell's connectivity analysis. In order to explain the connectivity between grains, A_F values are estimated for the M6B and M7B samples and tabulated in Table IV. The estimated A_F values were 4.62 and 1.86 for the M6B and M7B samples, respectively. According to Rowell's connectivity analysis, the higher A_F value is related to the better connectivity between grains. The estimated A_F value of the M6B sample was obtained higher than M7B sample. This result indicates the better intergranular connection in MgB_2 grains for the M6B sample. In addition, the RRR defined by $\rho_{300\,K}/\rho_{40\,K}$ was also estimated. Table IV illustrates $\rho_{40\,K}$, $\rho_{300\,K}$, $\Delta\rho$ ($\rho_{300\,K} - \rho_{40\,K}$), and RRR values for M6B and M7B samples. The room temperature resistivity value of the M6B sample was obtained lower than M7B sample. This is related to the better crystallinity of MgB_2 phase due to grain growth for the M6B sample.

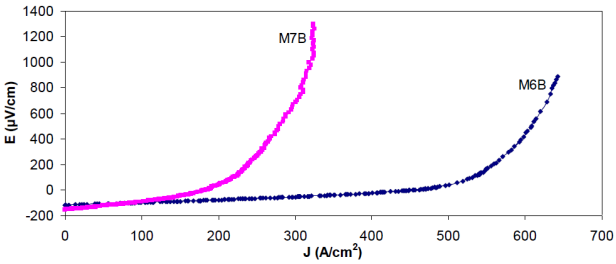

Fig. 6. Electric field versus current density graphs of the samples M6B and M7B (20 K).

TABLE IV

Values of the resistivity at 40 and 300 K ($\rho_{40\,K}$, $\rho_{300\,K}$), the resistivity difference ($\Delta\rho$), the RRR and the active cross-section area fraction (A_F) for the M6B and M7B samples.

Samples	$\rho_{40\,K}$ [$\mu\Omega$ cm]	$\rho_{300\,K}$ [$\mu\Omega$ cm]	$\Delta\rho(\rho_{300\,K} - \rho_{40\,K})$ [$\mu\Omega$ cm]	RRR	A_F [%]
M6B	0.81	2.39	1.58	2.95	4.62
M7B	1.97	5.98	4.01	3.03	1.86

The current–voltage (I–V) characteristic of the samples M6B and M7B were measured at 20 K with the standard four-probe method under self-field. Figure 6 shows the electric field as a function of transport critical current density for the samples M6B and M7B measured at 20 K. The transport critical current density values of

the samples M6B and M7B calculated from I–V measurements were found to be 450 A/cm^2 and 190 A/cm^2, respectively.

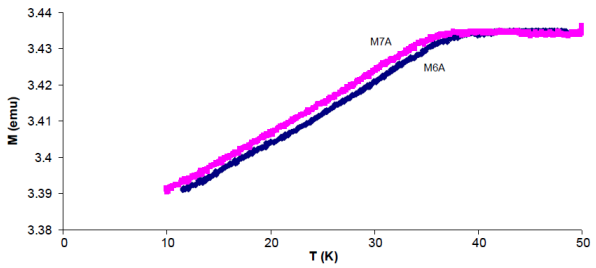

Fig. 7. Magnetic moment versus temperature graphs of the samples M6B and M7B.

Figure 7 shows the temperature dependence of magnetic moment for the samples M6B and M7B measured at 20 K. The offset superconducting transition temperature values of the MgB_2/Fe/Cu 6 and 7 filaments tapes were determined as 36.8 K and 36.6 K, respectively. These inductive superconducting transition temperature values are consistent with transport measurements of the MgB_2/Fe/Cu 6 and 7 filaments tapes.

4. Conclusions

The multifilamentary (6 and 7) MgB_2/Fe/Cu tapes were fabricated by *ex situ* PIT method using commercially available MgB_2 powder (Alfa Aesar, −325 mesh, < 44 μm) without any intermediate annealing. These samples were characterized using XRD, SEM, EDS, optical microscope, magnetic and transport measurements. In order to explain the connectivity between grains, A_F values are estimated for the M6B and M7B samples. The estimated A_F value of the sample M6B is higher than that of sample M7B. This result indicates the better intergranular connection in MgB_2 grains for the samples M6B. The room temperature resistivity value of the samples M6B was obtained lower than that of sample M7B. This is related to the better crystallinity of MgB_2 phase due to grain growth for the samples M6B. The transport J_c values of the samples M6B and M7B were obtained as 450 A/cm^2 and 190 A/cm^2 at 20 K, respectively. The offset superconducting transition temperature values of the MgB_2/Fe/Cu 6 and 7 filaments tapes were determined as 36.8 K and 36.6 K from the M−T graphs.

Acknowledgments

This work is financially supported by the National Boron Research Institute (BOREN) (project no. 2006--22-Ç21-15) and partly by the Scientific and Technological Research Council of Turkey (TUBITAK) (project no. 108M201), and partly by the Turkish State Planning Organization (DPT) (project no. 2004K120200).

References

[1] J. Nagamatsu, N. Nakagawa, T. Muranaka, Y. Zenitani, J. Akimitsu, *Nature* **410**, 63 (2001).

[2] C. Buzea, T. Yamashita, *Supercond. Sci. Technol.* **14**, R115 (2001).

[3] H. Xiao, W.H. Song, J.J. Du, Y.P. Sun, J. Fang, *Physica C* **386**, 593 (2003).

[4] S. Zhou, A.V. Pan, H. Liu, S. Dou, *Physica C* **382**, 349 (2002).

[5] Y. Feng, G. Yan, Y. Zhao, P.X. Zhang, E. Mossang, A. Sulpice, L. Zhou, *Physica C* **426-431**, 1216 (2005).

[6] H.L. Suo, C. Beneduce, X.D. Su, R. Flükiger, *Supercond. Sci. Technol.* **15**, 1058 (2002).

[7] C.M. Lee, J.H. Park, S.M. Hwang, J.H. Lim, J. Joo, W.N. Kang, C.J. Kim, *Physica C* **469**, 1527 (2009).

[8] V. Braccini, A. Malagoli, A. Tumino, M. Vignolo, C. Bernini, C. Fanciulli, G. Romano, M. Tropeano, A.S. Siri, G. Grasso, *IEEE Trans. Appl. Supercond.* **17**, 2 (2007).

[9] A. Malagoli, V. Braccini, M. Tropeano, M. Vignolo, C. Bernini, C. Fanciulli, G. Romano, M. Putti, C. Ferdeghini, E. Mossang, A. Polyanskii, D.C. Larbalestier, *J. Appl. Phys.* **104**, 103908 (2008).

[10] E. Yucel, C. Terzioglu, A. Varilci, I. Belenli, *J. Mater. Sci. Mater. Electron*, doi:10.1007/s10854-010-0274-9 (2010).

[11] T. Machi, S. Shimura, N. Koshizuka, M. Murakami, *Physica C* **392-396**, 1039 (2003).

[12] S. Shimura, T. Machi, K. Nakao, N. Koshizuka, S. Tanaka, K. Mochizuki, N. Shibata, K. Ushio, *Physica C* **426-431**, 1254 (2005).

[13] A. Asthana, A. Matsumoto, H. Kitaguchi, Y. Matsui, T. Hara, K. Watanabe, H. Yamada, N. Uchiyama, H. Kumakura, *Supercond. Sci. Technol.* **21**, 115013 (2008).

[14] S. Hata, T. Yoshidome, H. Sosiati, Y. Tomokiyo, N. Kuwano, A. Matsumoto, H. Kitaguchi, H. Kumakura, *Supercond. Sci. Technol.* **19**, 161 (2006).

[15] B.Q. Fu, Y. Feng, G. Yan, C.F. Liu, L. Zhou, L.Z. Cao, K.Q. Ruan, X.G. Li, *Physica C* **392-396** 1035 (2003).

[16] E. Ban, R. Sakaguchi, Y. Matsuoka, T. Goto, K. Watanabe, G. Nishijima, *Physica C* **426-431**, 1249 (2005).

[17] S.I. Schlachter, A. Frank, B. Ringsdorf, H. Orschulko, B. Obst, B. Liu, W. Goldacker, *Physica C* **445-448**, 777 (2006).

[18] S. Soltanian, X.L. Wang, J. Horvat, A.H. Li, H.K. Liu, S.X. Dou, *Physica C* **382**, 187 (2002).

[19] S. Soltaniana, X.L. Wanga, A.H. Li, E.W. Collings, M.D. Sumption, E. Lee, H.K. Liu, S.X. Dou, *Solid State Commun.* **124**, 59 (2002).

[20] K. Togano, J.M. Hur, A. Matsumoto, H. Kumakura, *Supercond. Sci. Technol.* **22**, 015003 (2009).

[21] M. Fu, J. Chen, Z. Jiao, H. Kumakura, K. Togano, L. Ding, Y. Zhang, Z. Chen, H. Han, J. Chen, *Physica C* **406**, 53 (2004).

[22] S.I. Schlachter, A. Frank, B. Ringsdorf, H. Orschulko, B. Obst, B. Liu, W. Goldacker, *Physica C* **445-448**, 777 (2006).

[23] K. Tanaka, M. Okada, M. Hirakawa, H. Yamada, H. Kumakura, H. Kitaguchi, *IEEE Trans. Appl. Supercond.* **14**, 2 (2004).

[24] K. Tanaka, H. Kitaguchi, H. Kumakura, H. Yamada, M. Hirakawa, M. Okada, *Supercond. Sci. Technol.* **18**, 678 (2005).

[25] E.W. Collings, E. Lee, M.D. Sumption, M. Tomsic, X.L. Wang, S. Soltanian, S.X. Dou, *Physica C* **386**, 555 (2003).

[26] K. Yamamoto, K. Osamura, S. Balamurugan, T. Nakamura, T. Hoshino, I. Muta, *Supercond. Sci. Technol.* **16**, 1052 (2003).

[27] K.Q. Ruan, H.L. Li, Y. Yu, C.Y. Wang, L.Z. Cao, C.F. Liu, S.J. Du, G. Yan, Y. Feng, X. Wu, J.R. Wang, X.H. Liu, P.X. Zhang, X.Z. Wu, L. Zhou, *Physica C* **386**, 578 (2003).

[28] X.L. Wang, S. Soltanian, J. Horvat, A.H. Liu, M.J. Qin, H.K. Liu, S.X. Dou, *Physica C* **361**, 149 (2001).

[29] S. Balamurugan, T. Nakamura, K. Osamura, I. Muta, T. Hoshino, *Physica C* **412-414**, 1184 (2004).

[30] J.M. Rowell, *Supercond. Sci. Technol.* **16**, R17 (2003).

[31] R.H.T. Wilke, S.L. Budko, P.C. Canfield, D.K. Finnemore, R.J. Suplinskas, S.T. Hannahs, *Physica C* **424**, 1 (2005).

[32] J. Jiang, B.J. Senkowicz, D.C. Larbalestier, E.E. Hellstrom, *Supercond. Sci. Technol.* **19**, L33 (2006).

[33] X. Xu, J.H. Kim, S.X. Dou, S. Choi, J.H. Lee, H.W. Park, M. Rindfleish, M. Tomsic, *J. Appl. Phys.* **105**, 103913 (2009).

[34] B.D. Cullity, *Element of X-ray Diffraction*, Addition--Wesley, Reading (MA) 1978.